Phenylalanine Dehydrogenase from *Rhodococcus sp.* M4: High-Resolution X-ray Analyses of Inhibitory Ternary Complexes Reveal Key Features in the Oxidative Deamination Mechanism[†,‡]

Janeen L. Vanhooke,[*,§] James B. Thoden,[§] Norbert M. W. Brunhuber,[||] John S. Blanchard,[⊥] and Hazel M. Holden[*,§]

Department of Biochemistry, University of Wisconsin—Madison, 1710 University Avenue, Madison, Wisconsin, 53705, Geo-Centers, Inc., Mt. Arlington, New Jersey 07856, and Department of Biochemistry, Albert Einstein College of Medicine, 1300 Morris Park Avenue, Bronx, New York 10461

Received September 17, 1998; Revised Manuscript Received November 17, 1998

ABSTRACT: The molecular structures of recombinant L-phenylalanine dehydrogenase from *Rhodococcus sp.* M4 in two different inhibitory ternary complexes have been determined by X-ray crystallographic analyses to high resolution. Both structures show that L-phenylalanine dehydrogenase is a homodimeric enzyme with each monomer composed of distinct globular N- and C-terminal domains separated by a deep cleft containing the active site. The N-terminal domain binds the amino acid substrate and contributes to the interactions at the subunit:subunit interface. The C-terminal domain contains a typical Rossmann fold and orients the dinucleotide. The dimer has overall dimensions of approximately 82 Å × 75 Å × 75 Å, with roughly 50 Å separating the two active sites. The structures described here, namely the enzyme·NAD^+·phenylpyruvate, and enzyme·NAD^+·β-phenylpropionate species, represent the first models for any amino acid dehydrogenase in a ternary complex. By analysis of the active-site interactions in these models, along with the currently available kinetic data, a detailed chemical mechanism has been proposed. This mechanism differs from those proposed to date in that it accounts for the inability of the amino acid dehydrogenases, in general, to function as hydroxy acid dehydrogenases.

The amino acid dehydrogenases are a widely distributed family of enzymes that catalyze the oxidative deamination of an amino acid to its keto acid and ammonia with the concomitant reduction of $NAD(P)^+$.[1] These enzymes have been the object of mechanistic investigations for over three decades (*1*) and, more recently, the subject of numerous three-dimensional X-ray crystallographic analyses. The first molecular model to be reported for an amino acid dehydrogenase was that of the hexameric L-glutamate dehydrogenase from *Clostridium symbiosum* (*2*). As observed in other NAD^+-dependent dehydrogenases, the three-dimensional fold of each monomer was shown to be distinctly bilobal with a deep cleft separating the N- and C-terminal domains. An X-ray analysis of crystals soaked in a solution of NAD^+ revealed that the C-terminal domain was responsible for positioning the dinucleotide cofactor and contained a modified "Rossmann" fold (*3*) with seven rather than six strands of β-sheet and one of the strands running in the reverse direction. In a subsequent study (*4*), the X-ray structure of the enzyme−glutamate complex revealed the residues involved in amino acid positioning as well as the large conformational change associated with substrate binding. Following this elegant work on glutamate dehydrogenase, the three-dimensional structure of the octameric *Bacillus sphaericus* L-leucine dehydrogenase was determined and allowed a detailed comparison to be made between the two enzymes (*5*). The three-dimensional structure of a third amino acid dehydrogenase, the dimeric meso-diaminopimelate dehydrogenase from *Corynebacterium glutamicum*, was subsequently reported (*6*). This enzyme uniquely acts on a D-amino acid center of its symmetric diamino acid substrate and, in addition, the N- rather than C-terminal domain adopts the Rossmann fold. Most recently reported were structures of the hexameric L-alanine dehydrogenase from the cyanobacterium *Phormidium lapideum*, alone and in binary complexes with either NAD^+ or pyruvate (*7*). This enzyme shares little primary structural homology with other members of the amino acid dehydrogenase family and is unique among them in catalyzing transfer of the 4R rather than the 4S hydrogen of NADH. While all of the above-mentioned X-ray crystallographic investigations have provided enormous amounts of new information regarding these fascinating enzymes, to date there are no reported structures of ternary complexes of amino acid dehydrogenases. Indeed, the structural studies of such ternary complexes are critical for a more complete understanding of catalysis by this family of enzymes.

[†] This research was supported in part by grants from the NIH (DK47814 to H.M.H.) and (GM 33449 to J.S.B.), and the NSF (BIR-9317398).

[‡] X-ray coordinates have been deposited in the Brookhaven Protein Data Bank (1bwg and 1bxg) and will be released upon publication .

* To whom correspondence should be addressed.

[§] University of Wisconsin—Madison.

[||] Geo-Centers.

[⊥] Albert Einstein College of Medicine.

[1] Abbreviations: NAD^+, oxidized nicotinamide adenine dinucleotide; NADH, reduced nicotinamide adenine dinucleotide; IPTG, isopropyl-thio-β-D-galactoside; CHES, 2-(*N*-cyclohexylamino)ethanesulfonic acid; LB, Luria-Bertani; SDS−PAGE, sodium dodecyl sulfate polyacrylamide gel electrophoresis; BCA, bicinchoninic acid; BSA, bovine serum albumin.

10.1021/bi982244q CCC: $18.00
Published on Web 02/03/1999

Scheme 1

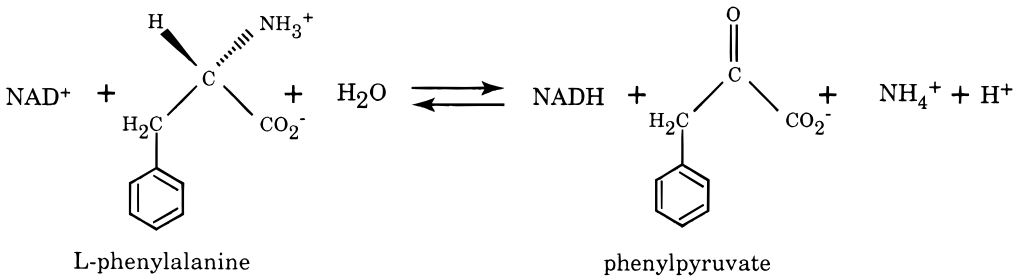

Here, we describe the molecular structures of two inhibitory ternary complexes of phenylalanine dehydrogenase from *Rhodococcus sp.* M4. This enzyme catalyzes the reversible NAD^+-dependent oxidative deamination of L-phenylalanine to generate phenylpyruvate and ammonia as shown in Scheme 1.

From the studies of N.M.W. Brunhuber and J.S. Blanchard (manuscript in preparation), it is known that the catalytic mechanism of the enzyme is ordered Bi−Ter with NAD^+ binding first, followed by L-phenylalanine. Products are released in the order of NH_4^+, phenylpyruvate, and NADH. L-Phenylalanine dehydrogenase is a *B*-side specific enzyme and transfers the 4S hydrogen of NADH to the imine of phenylpyruvate in the reverse reaction shown in Scheme 1.

The protein has been cloned and sequenced, and the 356 amino acid enzyme expressed in *Escherichia coli*, which naturally lacks this enzyme (*8*). Interestingly, the *Rhodococcus* phenylalanine dehydrogenase is most similar to the *Bacillus stearothermophilus* leucine dehydrogenase (39% sequence identity), followed by the other phenylalanine dehydrogenases, thus suggesting a common amino acid dehydrogenase ancestor that acted upon both aromatic and aliphatic amino acids (*8*). In the present investigation, we describe the crystallizations and structural analyses of the phenylalanine dehydrogenase·NAD^+·phenylpyruvate and the phenylalanine dehydrogenase·NAD^+·β-phenylpropionate ternary complexes to 1.5 and 2.3 Å resolution, respectively. The structural studies of these inhibitory complexes [β-phenylpropionate is a competitive inhibitor of both the forward and reverse reactions (N.M.W. Brunhuber and J.S. Blanchard, manuscript in preparation)] have allowed for a detailed understanding of the active-site geometry for phenylalanine dehydrogenase and have also provided molecular insight into why these enzymes, in general, do not function as hydroxy acid dehydrogenases.

MATERIALS AND METHODS

Materials. Bacto tryptone and bacto yeast extract were products of Difco Labs (Detroit, MI). IPTG was purchased from Fisher Scientific (Pittsburgh, PA). Q-Sepharose Fast Flow was obtained from Pharmacia (Uppsala, Sweden). Sodium monobasic phosphate, potassium dibasic phosphate, and sodium chloride were purchased from Mallinckrodt (Paris, KY). CHES was obtained from Research Organics (Cleveland, OH). All other reagents were products of Sigma (St. Louis, MO) and Aldrich (Milwaukee, WI) chemical companies.

Cell Culture and Protein Overexpression. *E. coli* BL21-(DE3) pBL-1B cells were cultured in LB medium supplemented with ampicillin at 200 μg/mL. A 200 mL culture (7−8 h old) was diluted 100-fold into 6 L of medium in baffled culture flasks (500 mL/2 L flask) and shaken at 37 °C until $A_{600} \approx 1.0$. The culture was then chilled to approximately 23 °C by swirling the flasks, four at a time, in an ice−water bath for 2 min. Sterile IPTG was added to a final concentration of 0.005 mM and shaking resumed at 23 °C for 8 h. The cells were harvested by centrifugation at 4400*g* for 10 min, and the cell paste was scooped into liquid nitrogen, weighed, and stored at −80 °C.

All purification procedures were performed at 4 °C. An extract free of cell debris and nucleic acids was prepared from the frozen cells (42−48 g) (N.M.W. Brunhuber and J.S. Blanchard, manuscript in preparation). The extract was applied to a 5.0 × 20 cm column of Q-Sepharose Fast Flow and eluted with a 3 L gradient of NaCl that increased linearly from 0.2 to 1.0 M in 20 mM triethanolamine, pH 7.8. Phenylalanine dehydrogenase emerged from the column at approximately 550 mM NaCl and was pooled based on SDS−PAGE analysis of the fractions. The pooled protein was dialyzed against 12 L of 20 mM triethanolamine, pH 7.8, containing 50 mM NaCl for 4 h and then applied to a 2.1 × 23 cm column of Q-Sepharose Fast Flow. The enzyme was eluted from the second Q-Sepharose column with an 800 mL gradient of NaCl that increased linearly as described for the first column. Fractions judged to be at least 98% pure by SDS−PAGE were pooled, concentrated by ultrafiltration (Amicon stirred cell, YM30 membrane), and dialyzed against 50 mM triethanolamine, pH 7.8, containing 100 mM NaCl (buffer A). The protein concentration was adjusted to 10 mg/mL by addition of either buffer A or buffer A plus NAD^+, for a final concentration of 10 mM NAD^+ in the NAD^+-containing fraction. Aliquots were quickly frozen in liquid nitrogen and stored at −80 °C.

Protein concentration was determined by the BCA protein assay of Pierce (Rockford, IL), with BSA as a standard. Enzymatic activity was determined spectrophotometrically from the initial rate of NADH formation at 340 nm in the presence of 10 mM NAD^+ and 20 mM L-phenylalanine at pH 8.0 (100 mM triethanolamine) and 27 °C. Roughly 120 mg of pure enzyme with a specific activity of 46−49 units/mg was obtained from each purification (one unit is defined to catalyze the oxidative deamination of 1 μmol of L-phenylalanine to phenylpyruvate per minute under the conditions above).

Crystallization of the Enzyme·NAD^+·Phenylpyruvate Complex. Crystallization trials of L-phenylalanine dehydrogenase were conducted by the hanging drop method of vapor diffusion in the presence and absence of added substrates using a sparse matrix sampling technique. These trials were conducted at both 4 °C and room temperature (~22 °C).

L-Phenylalanine dehydrogenase was observed to crystallize under a variety of conditions. The crystal form employed for the structural analysis described here was grown at room temperature by macroseeding into small batch setups as follows: a 7.5 mg/mL solution of L-phenylalanine dehydrogenase in buffer A containing 10 mM NAD^+ and 10 mM phenylpyruvate was quickly mixed with an equal volume of precipitant solution composed of 2.6 M Na^+/K^+ phosphate, 100 mM CHES (pH 8.7), and 4% (v/v) 2-propanol. Drops of 20 μL were pipetted into greased 9-well Plexiglas depression plates and were carefully seeded thereafter with small crystals produced in previous batch experiments. The crystals grew as rectangular, bladed tablets and achieved typical dimensions of 0.4 mm × 0.2 mm × 0.2 mm within 3−6 days.

Preparation of Heavy Atom Derivatives and X-ray Data Collection and Processing for the Enzyme·NAD⁺·Phenylpyruvate Complex. Precession photography of the *hk*0 and *h*0*l* zones revealed that the crystals belonged to the orthorhombic space group $P2_12_12_1$, with unit cell dimensions of $a = 65.3$ Å, $b = 111.6$ Å, and $c = 116.8$ Å and two subunits per asymmetric unit.

Crystals employed for collection of the native X-ray data set were transferred to a synthetic mother liquor containing 1.6 M Na^+/K^+ phosphate, 50 mM CHES (pH 8.7), 2% (v/v) 2-propanol, 5 mM NAD^+, and 5 mM phenylpyruvate and soaked for 2 days prior to X-ray exposure. Heavy atom derivative crystals were prepared by direct transfer from the batch experiments to the above synthetic mother liquor containing the desired heavy atom compound. Three isomorphous heavy atom derivatives were prepared by soaking the crystals in 1.0 mM K_2PtCl_4, 6.4 mM $KAu(CN)_2$, or 10.0 mM $K_2Pt(CN)_6$.

The crystals were mounted in quartz capillary tubes and cooled to −2.5 °C for X-ray data collection. The initial native X-ray data set was collected to 2.7 Å resolution from two crystals with a Bruker AXS Inc. HiStar area detector system. The X-ray source was Ni-filtered Cu Kα radiation from a Rigaku RU200 X-ray generator operated at 50 mV and 90 mA and equipped with double focusing mirrors. The crystal-to-detector distance was 15 cm, with a step size of 0.15° per frame. X-ray data sets for the $KAu(CN)_2$ and $K_2Pt(CN)_6$ derivatives were collected to 3.3 Å resolution from single crystals. The X-ray data set for the K_2PtCl_4 derivative was collected to 2.7 Å resolution from two crystals, and Friedel pairs were measured for all reflections in this particular data set.

The X-ray data sets were processed with the data reduction software package XDS (*9*, *10*) and internally scaled with the program XCALIBRE (G. Wesenberg and I. Rayment, unpublished software). Relevant X-ray data collection statistics are given in Table 1. The native X-ray data set was 97% complete to 2.7 Å resolution. The heavy atom derivative data sets were scaled to the native by a "local" scaling procedure developed by Drs. G. Wesenberg, W. Rypniewski, and I. Rayment. The R_{factor}s (based on amplitudes) between the native and K_2PtCl_4, $K_2Pt(CN)_6$, and $KAu(CN)_2$ X-ray data sets were 18.2, 16.0, and 18.6%, respectively.

After the structure was solved to 2.8 Å resolution, a high-resolution native X-ray data set to 1.5 Å resolution was collected from a single crystal at −160 °C at the Structural Biology Center Beamline 19-ID located at the Advanced Photon Source. The X-ray data were measured with radiation of wavelength 1.033 Å using the SBC APS1 3 × 3 CCD array detector positioned at a distance of 125 mm. A total of 275 frames was collected with an oscillation angle of 0.40° and an exposure time of 5 s/frame. The raw frames were corrected (courtesy of Dr. Frank Rotella, Advanced Photon Source) and subsequently converted into "Bruker" format with the program FRM2FRM (supplied by Dr. Kingsley Smith, Bruker AXS Inc.). The data were then indexed with SMART2K (Bruker AXS Inc.), processed with SAINT2K (Bruker AXS Inc.), and finally scaled with XCALIBRE (G. Wesenberg and I. Rayment, unpublished software). Relevant X-ray data collection statistics for this data set are also given in Table 1.

Structural Determination and Least-Squares Refinement of the Enzyme·NAD⁺·Phenylpyruvate Complex. The positions of the heavy atom binding sites were determined by inspection of appropriate difference Patterson maps calculated from 30 to 5.0 Å resolution. The K_2PtCl_4, $K_2Pt(CN)_6$, and $KAu(CN)_2$ derivatives contained 4, 2, and 1 binding sites, respectively. The heavy atom derivatives were placed on a common origin by difference Fourier maps and the positions and occupancies for each heavy atom binding site were refined by the origin-removed Patterson-function correlation method to 2.8 Å resolution (*11*, *12*). Protein phases were calculated with the program HEAVY (*12*), and relevant phase calculation statistics can be found in Table 2.

An electron density map calculated to 2.8 Å resolution clearly revealed the molecular boundaries for the dimer in the asymmetric unit. The map was further improved by molecular averaging and solvent flattening (*13*). From this averaged electron density map, a complete model of the enzyme was built. The model was then placed back into the unit cell and subjected to alternate cycles of least-squares refinement with the program TNT at 2.8 Å and then at 1.5 Å resolution (*14*). Relevant refinement statistics are presented in Table 3.

A Ramachandran plot for all main-chain dihedral angles is depicted in Figure 1. The only significant outlier is Ala 239 in each subunit. Ala 239 adopts these strained dihedral angles due to a hydrogen bond between its carbonyl oxygen and the 3′-hydroxyl group of the nicotinamide ribose of NAD^+. The following amino acid residues were modeled into the electron density in alternate conformations: Asp 9, Thr 54, Asp 55, Met 74, Ser 89, Asp 91, Ser 110, Ser 123, and Asn 262 in subunit I and Asp 55, Thr 246, Ser 255, and Ser 306 in subunit II. Since the electron density was rather weak in subunit II for the nicotinamide nucleoside portion of NAD^+, only the ADP portion of the dinucleotide cofactor was included in the refinement.

Structural Determination of the Enzyme·NAD⁺·β-Phenylpropionate Complex. For crystallization of this inhibitory complex, a 7.5 mg/mL solution of L-phenylalanine dehydrogenase in buffer A containing 10 mM NAD^+ was quickly mixed with an equal volume of a precipitant solution composed of 2.70 M Na^+/K^+ phosphate, 100 mM CHES (pH 8.7), 10 mM β-phenylpropionate, and 4% (v/v) 2-propanol. Drops of 20 μL were pipetted into greased 9-well Plexiglas depression plates and were carefully seeded thereafter with small crystals produced in previous batch experiments. The crystals grew as rectangular bipyramids and achieved typical dimensions of 0.4 mm × 0.2 mm ×

Table 1: Intensity Statistics

	resolution range (Å)								
	overall	100−5.40	4.29	3.74	3.40	3.16	2.97	2.82	2.70
enzyme·NAD^+·phenylpyruvate complex									
observations	72 587	13 094	12 399	10 894	9738	8624	7536	6130	4172
independent reflections	23 408	3171	3054	3019	2938	2981	2931	2831	2438
completeness (%)	97.0	99.6	99.9	100.0	99.7	99.9	99.0	95.2	82.5
avg I/avg σ (I)	6.9	15.7	11.0	7.7	5.7	3.9	3.0	2.4	2.0
R_{factor} (%)[a]	6.1	3.2	4.0	5.7	7.5	10.1	12.6	15.9	18.4
K_2PtCl_4									
observations	70 939	12 721	11 949	10 666	9441	8251	7189	6020	4702
independent reflections	23 469	3164	3003	2964	2918	2898	2858	2856	2808
avg I/avg σ (I)	6.6	15.6	10.6	7.2	5.2	3.4	2.7	2.3	1.8
R_{factor} (%)[a]	6.4	3.3	4.2	6.0	8.0	11.7	14.3	17.1	20.6
$KAu(CN)_2$									
observations	23 824	6552	5666	4802	4023	2548	233		
independent reflections	13 503	3091	2925	2739	2561	1968	219		
avg I/avg σ (I)	6.2	11.9	7.7	5.2	3.9	2.6	2.2		
R_{factor} (%)[a]	8.7	5.1	7.7	11.2	13.8	18.2	12.6		
$K_2Pt(CN)_6$									
observations	25 019	6821	5971	5086	4243	2676	222		
independent reflections	13 858	3044	3000	2888	2679	2044	203		
avg I/avg σ (I)	5.8	11.3	7.2	4.7	3.5	2.4	2.2		
R_{factor} (%)[a]	7.7	4.6	6.5	9.8	13.0	17.3	23.5		

High-Resolution Native X-ray Data for the Enzyme·NAD^+·Phenylpyruvate Complex

	resolution range (Å)								
	overall	30.0−3.00	2.38	2.08	1.89	1.75	1.65	1.57	1.50
no. of measurements	461 544	52 247	60 751	62 394	64 299	67 016	60 402	53 240	41 195
no. of independent reflections	121 716	16 706	16 143	15 898	15 791	15 574	14 850	14 123	12 631
% completeness	94	100	99	99	98	93	95	91	77
avg I/avg σ (I)	12.3	58.5	18.9	12.9	8.4	5.1	3.4	2.7	2.3
R_{factor} (%)[a]	8.0	3.6	6.8	9.0	12.9	15.1	17.3	20.3	23.6

High-Resolution Native X-ray Data for the Enzyme·NAD^+·β-Phenylpropionate Complex

	resolution range (Å)								
	overall	30.0−4.60	3.65	3.19	2.90	2.69	2.53	2.40	2.30
no. of measurements	73 548	14 428	13 246	11 139	9188	7792	6649	5986	5120
no. of independent reflections	34 077	4871	4738	4618	4463	4256	3961	3742	3428
% completeness	88	95	97	95	92	88	83	78	72
avg I/avg σ (I)	6.7	17.1	10.7	6.3	3.6	2.4	2.0	1.7	1.6
R_{factor} (%)[a]	7.2	3.6	5.4	8.1	12.3	17.1	20.0	22.3	24.6

[a] $R_{factor} = (\sum|I - \bar{I}|/\sum I) \times 100$.

Table 2: Phase Calculation Statistics

	resolution range (Å)							
	∞ − 9.52	6.08	4.77	4.05	3.59	3.25	2.99	2.79
no. of reflections	1237	1992	2497	2893	3194	3387	3442	3114
figure of merit	0.68	0.67	0.56	0.51	0.45	0.42	0.25	0.16
phasing power[a]								
K_2PtCl_4								
centric reflections	0.67	1.11	0.84	0.79	0.80	0.88	0.95	0.85
acentric reflections	0.96	1.60	1.27	1.16	1.10	1.22	1.11	0.94
$KAu(CN)_2$								
centric reflections	1.26	1.35	0.96	0.88	0.87	0.81		
acentric reflections	1.59	1.56	1.12	0.98	1.05	1.10	0.85	
$K_2Pt(CN)_6$								
centric reflections	0.80	0.85	0.75	0.73	0.61	0.70	0.38	
acentric reflections	1.21	1.25	1.06	0.98	0.88	0.82	0.70	

[a] Phasing power is the ratio of the root-mean-square heavy-atom scattering factor amplitude to the root-mean-square lack of closure error.

0.3 mm within 3−6 days. These crystals also belonged to orthorhombic space group $P2_12_12_1$, with unit cell dimensions of $a = 65.5$ Å, $b = 111.6$ Å, and $c = 117.0$ Å and a dimer in the asymmetric unit.

For X-ray data collection, the crystals were transferred to a synthetic mother liquor containing 1.68 M Na^+/K^+ phosphate, 50 mM CHES (pH 8.7), 2% (v/v) 2-propanol, 5 mM NAD^+, and 20 mM β-phenylpropionate and soaked for 2 days prior to X-ray exposure. The X-ray data set was recorded from a single crystal on a Bruker AXS Inc. HiStar area detector system at −3.0 °C with Ni-filtered Cu Kα radiation from a Rigaku RU200 X-ray generator operated at 50 mV and 90 mA and equipped with a 300 μm focal cup and Göbel focusing mirrors. The data set was collected at a crystal-to-detector distance of 12 cm in frames of 0.15° angular width. The data were processed with XDS and

Table 3: Least-Squares Refinement Statistics for the Phenylalanine Dehydrogenase Complexes

	phenylpyruvate	β-phenylpropionate
resolution limits (Å)	30.0−1.5	30.0−2.3
R_{factor} (%)[a]	19.5	17.0
no. of reflections used	120 793	34 077
no. of protein atoms	5167	5137
no. of solvent atoms[b]	1058	181
weighted root-mean-square deviations from ideality		
bond length (Å)	0.013	0.014
bond angle (deg)	2.23	2.49
planarity (trigonal) (Å)	0.005	0.008
planarity (other planes) (Å)	0.012	0.009
torsional angle (deg)[c]	14.8	16.0

[a] $R_{factor} = \Sigma||F_o| - |F_c||/\Sigma|F_o|$, where F_o is the observed structure-factor amplitude and F_c is the calculated structure-factor amplitude. [b] These include 1071 water molecules, two sodium ions, two potassium ions, four isopropanols, three ethylene glycols, and one inorganic phosphate for the enzyme·NAD^+·phenylpyruvate complex and 175 water molecules, one potassium ion, and one inorganic phosphate for the enzyme·NAD^+·β-phenylpropionate complex. [c] The torsional angles were not restrained during the refinement.

internally scaled with XCALIBRE. Relevant data statistics are given in Table 1. The X-ray data set was 88% complete to 2.3 Å resolution.

The structure of the enzyme·NAD^+·β-phenylpropionate complex was solved by difference Fourier techniques starting with the enzyme·NAD^+·phenylpyruvate model in which the dinucleotide and substrate had been removed. Alternate cycles of model building and least-squares refinement reduced the R_{factor} to 17.0% for all measured X-ray data. Relevant refinement statistics are given in Table 3. The electron densities for the NAD^+ and the phenylpyruvate were clearly better ordered in subunit II. Again, the only significant outliers in the Ramachandran plot were alanines 239 in each subunit of the dimer.

RESULTS

Tertiary and Quaternary Structure. Phenylalanine dehydrogenase contains 356 amino acid residues. The N-terminal methionine is cleaved off the mature polypeptide chain, and thus the numbering employed in this paper refers to the N-terminal serine as position 1. Additionally, in both of the ternary complexes described here, namely the enzyme·NAD^+·phenylpyruvate and the enzyme·NAD^+·β-phenylpropionate species, there are two subunits per asymmetric unit. For the sake of simplicity, however, only the molecular motifs of one of the subunits will be described for each of the ternary complexes unless otherwise noted. For the enzyme·NAD^+·phenylpyruvate complex, the first subunit in the asymmetric unit will be discussed, whereas in the enzyme·NAD^+·β-phenylpropionate complex, the second subunit will serve as the focus. The reason for these choices is simply because these specific subunits were better ordered than the others in the crystalline lattice. However, it should be noted that for the enzyme·NAD^+·phenylpyruvate homodimer, all backbone atoms between the two subunits superimpose with a root-mean-square deviation of 0.81 Å, and for the enzyme·NAD^+·β-phenylpropionate dimeric species, these atoms correspond with a root-mean-square deviation of 0.83 Å.

A ribbon representation of one subunit of the enzyme·NAD^+·phenylpyruvate abortive complex is displayed in Figure 2a, and a list of the secondary structural elements given in Table 4. The subunit is composed of two distinct structural N- and C-domains defined by Ser 1 to Gly 145 and Ala 146 to Ser 349, respectively. These domains are involved in binding the amino (or keto) acid substrate and the dinucleotide, respectively. No electron density was observable for residues Thr 350 to Ala 355. The N-terminal motif contains five β-strands that form a mixed β-sheet with the overall topology shown in Figure 2b. These β-strands range in length from 5 to 11 amino acid residues with β-strand B displaying a distinct bulge at Asp 30 ($\phi = -70.9°$, $\psi = -49.6°$). In addition to these β-strands, there are four α-helices distributed as two on each side of the mixed β-sheet and ranging in length from 6 to 19 amino acid residues. The β-strands and α-helices are connected by various reverse

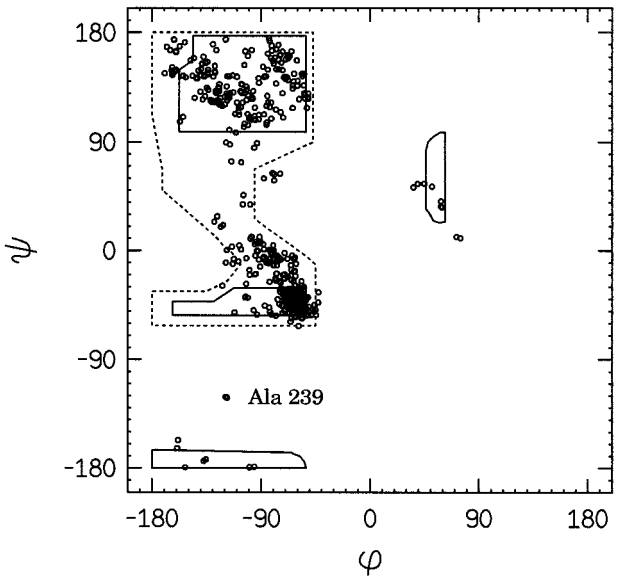

FIGURE 1: Ramachandran plot of all nonglycinyl main-chain dihedral angles. The torsional angles for both subunits in the asymmetric unit are indicated by the circles. Fully allowed ϕ,ψ values are enclosed by solid lines; those partially allowed are enclosed by dashed lines.

Table 4: List of Secondary Structural Elements

residue	type of structural element	residue	type of structural element
Ser 1−Leu 6	α-helix (A)	Thr 177−Gln 181	β-sheet (F)
Met 12−Asp 18	β-sheet (A)	Ala 185−Ala 194	α-helix (F)
Arg 19−Gly 22	type I turn	Ala 195−Gly 198	type I turn
Ala 23−Ser 31	β-sheet (B)	Gln 200−Asp 205	β-sheet (G)
Thr 32−Gly 35	type I turn	Thr 208−Ala 214	α-helix (G)
Pro 36−Tyr 46	β-sheet (C)	Val 215−Gly 218	type I turn
Leu 49−Met 67	α-helix (B)	Thr 220−Ala 223	β-sheet (H)
Ala 68−Asn 71	type I turn	Leu 224−Val 227	type I turn
Gly 75−Leu 83	β-sheet (D)	Asp 226−Ser 229	~type I turn
Pro 86−Ser 89	type III turn	Pro 231−Pro 237	β-sheet (I)
Pro 92−Ile 106	α-helix (C)	Thr 246−Arg 250	α-helix (H)
Asp 107−Ser 110	type I turn	Leu 252−Gly 259	β-sheet (J)
Leu 109−Asn 112	type I′ turn	Ala 261−Val 264	~type II turn
Tyr 113−Pro 117	β-sheet (E)	Glu 268−Leu 274	α-helix (I)
Asp 118−Thr 121	type II turn	His 275−Gly 278	type I turn
Ser 123−Thr 132	α-helix (D)	Ile 279−Pro 283	β-sheet (K)
Ser 140−Arg 143	type III turn	Asp 284−Glu 299	α-helix (J)
Leu 141−Gly 144	type I turn	Glu 305−Ser 326	α-helix (K)
Ala 150−Val 165	α-helix (E)	Asp 327−Gly 330	type I turn
Ala 166−Gly 169	type I turn	Pro 333−Ser 349	α-helix (L)
Leu 173−Leu 176	type II turn		

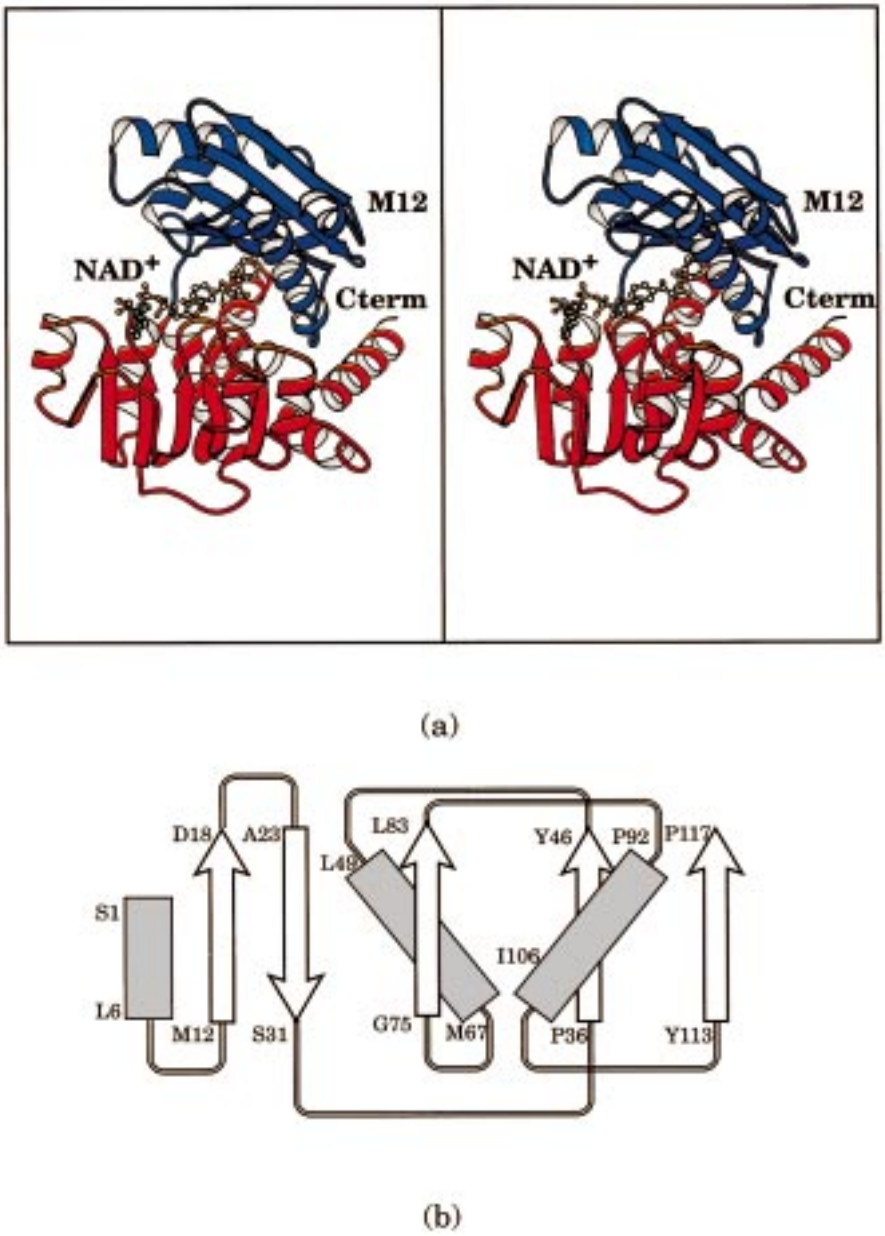

FIGURE 2: Ribbon representation of one subunit of the phenylalanine dehydrogenase·NAD^+·phenylpyruvate ternary complex. (a) The substrate binding domain is shown in blue while the dinucleotide binding motif is depicted in red. The NAD^+ and phenylpyruvate molecules are displayed in ball-and-stick representations. (b) The topology corresponding to the substrate binding domain is shown. Rectangles and arrows represent α-helices and β-strands, respectively.

turns as listed in Table 4. Strikingly, the topology of the N-terminal domain is nearly identical to that observed in leucine dehydrogenase (*5*). A search of the Brookhaven Protein Data Bank with the software Dejavu, however, failed to detect any other protein or domain with a similar three-dimensional motif (*15*).

As expected from amino acid sequence analyses, the C-terminal domain of L-phenylalanine dehydrogenase contains a classical "Rossmann" fold of six strands of parallel β-sheet flanked on either side by two and three α-helices. Like β-strand B, β-strands I and J are punctuated by bulges at Asp 233 ($\phi = -80.1°$, $\psi = -53.6°$) and Ser 255 ($\phi = -102.3°$, $\psi = -27.9°$), respectively. Following the dinucleotide-binding motif, the polypeptide chain folds into three α-helical regions that serve to close off one side of the active-site cleft, which is wedged between the N- and C-terminal motifs.

While initial biochemical studies suggested that L-phenylalanine dehydrogenase from *Rhodococcus sp.* M4 functions as a tetramer (N.M.W. Brunhuber and J.S. Blanchard, manuscript in preparation), the enzyme clearly packed in the $P2_12_12_1$ crystalline lattice as a dimer. Shown in Figure 3 is a ribbon representation of the enzyme·NAD^+·phenylpyruvate dimer which has overall dimensions of approximately 82 Å × 75 Å × 75 Å. The subunit:subunit interface is not very extensive, with approximately 1100 $Å^2$ of surface area lost upon dimerization, as calculated according to the method of Lee and Richards (*16*) with a probe sphere radius of 1.4 Å. As can be seen, the subunit:subunit interface is formed primarily, but not exclusively, by two strands of β-sheet running antiparallel and delineated by Met 12 to Asp 18. These secondary structural elements serve as a bridge to connect the five-stranded N-terminal β-sheets in each subunit, thereby forming a 10-stranded mixed β-sheet. The second

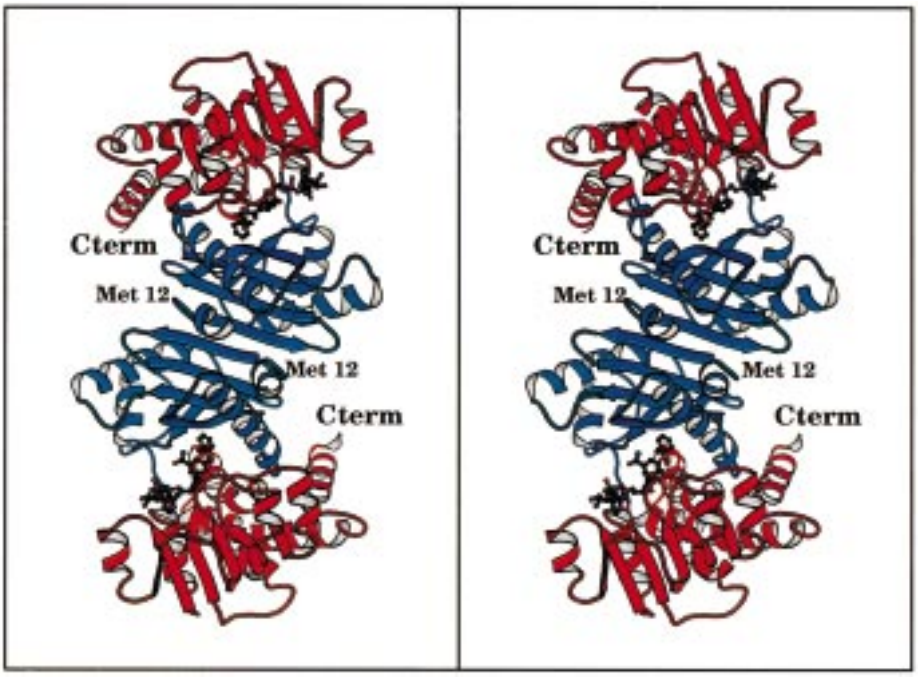

FIGURE 3: Ribbon representation of the complete phenylalanine dehydrogenase dimer with bound NAD^+ and phenylpyruvate. The active sites are separated by approximately 50 Å.

area of subunit:subunit contact occurs through the type I turns defined by Asp 107 to Ser 110.

Active Site for the Phenylalanine Dehydrogenase·NAD^+·Phenylpyruvate Ternary Complex. Electron densities corresponding to the oxidized dinucleotide and the phenylpyruvate moieties are displayed in Figure 4a. As can be seen, the nicotinamide ring adopts the anti- rather than the syn-conformation that would be expected for a *B*-side-specific enzyme. As a consequence of this arrangement, the distance between C4 of the nicotinamide ring and C^α of phenylpyruvate is approximately 4.9 Å. In addition, the carboxamide group of the dinucleotide is positioned very closely, within 2.8 Å in some cases, to atoms of the phenylpyruvate.

A close-up view of the active site with bound NAD^+ and phenylpyruvate is displayed in Figure 5a. For the collection of the higher resolution, low temperature, X-ray data set employed in this structural analysis, the crystals were transferred to a cryo-protectant solution containing ethylene glycol and, indeed, an ethylene glycol molecule is located in the active site as indicated in Figure 5a. In addition to the ethylene glycol, there are 12 water molecules positioned within the active-site region as indicated by the black spheres. A cartoon of the hydrogen-bonding interactions between the NAD^+, the phenylpyruvate, and the protein is depicted in Figure 5b. As one would expect for an enzyme that reversibly binds NAD(H), there are few specific interactions between the dinucleotide and the protein. Indeed, only two side chain functional groups are involved in hydrogen bonding to the NAD^+, namely the carboxylate group of Asp 205 and the guanidinium group of Arg 210, both of which serve to anchor, respectively, the 2′- and 3′-hydroxyl groups of the adenine ribose to the protein as indicated in Figure 5b. Additionally, there are two hydrogen bonds formed between the phosphoryl oxygens of the NAD^+ and the backbone amide groups of Ala 185 and Val 186. The 2′- and 3′-hydroxyl groups of the nicotinamide ribose lie within hydrogen-bonding distance to the backbone amide group of Asn 262 and the carbonyl group of Ala 239, respectively. Other than these specific protein:dinucleotide interactions, all other hydrogen-bonding interactions involving the dinucleotide cofactor are mediated through solvent molecules. With respect to phenylpyruvate binding, both Lys 66 and Lys 78 serve important structural roles by forming hydrogen-bonding interactions with one of the carboxylate oxygens and the keto oxygen of the ligand, respectively.

Active Site for the Phenylalanine Dehydrogenase·NAD^+·β-Phenylpropionate Ternary Complex. The overall molecular architecture of the phenylalanine dehydrogenase·NAD^+·β-phenylpropionate ternary complex is similar to that described above for the enzyme complexed with phenylpyruvate such that all polypeptide chain backbone atoms between the two models superimpose with a root-mean-square deviation of 0.82 Å. While the secondary and tertiary structures are similar, the conformation of the dinucleotides are strikingly different in these complexes as can been seen by the electron density displayed in Figure 4b. In the phenylalanine dehydrogenase·NAD^+·β-phenylpropionate ternary complex, the nicotinamide ring is rotated by approximately 180° about the glycosidic bond, thereby yielding the expected syn-conformation for *B*-side specific dehydrogenases. This type of conformational flipping of the nicotinamide ring relative to the ribose has been observed repeatedly in the structural analyses of UDP-galactose 4-epimerase from *E. coli*, where the position of this reactive group is dependent upon the identity of the ligand occupying the substrate-binding site and/or the oxidation state of the dinucleotide (*17*, *18*). In addition to this obvious difference in ring orientation, the conformation of the nicotinamide ribose in the phenylalanine dehydrogenase·NAD^+·β-phenylpropionate ternary complex changes from a $C_{3'}$-endo (as in the model with bound phenylpyruvate) to the more commonly observed $C_{2'}$-endo pucker. This change in ribose pucker creates interactions

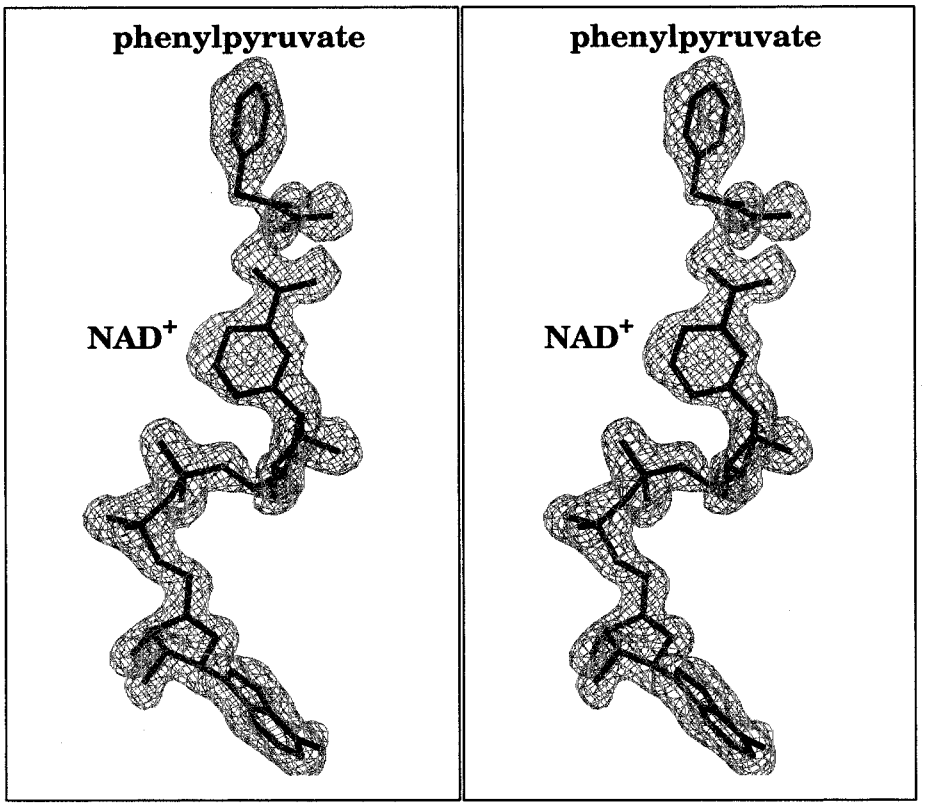

(a)

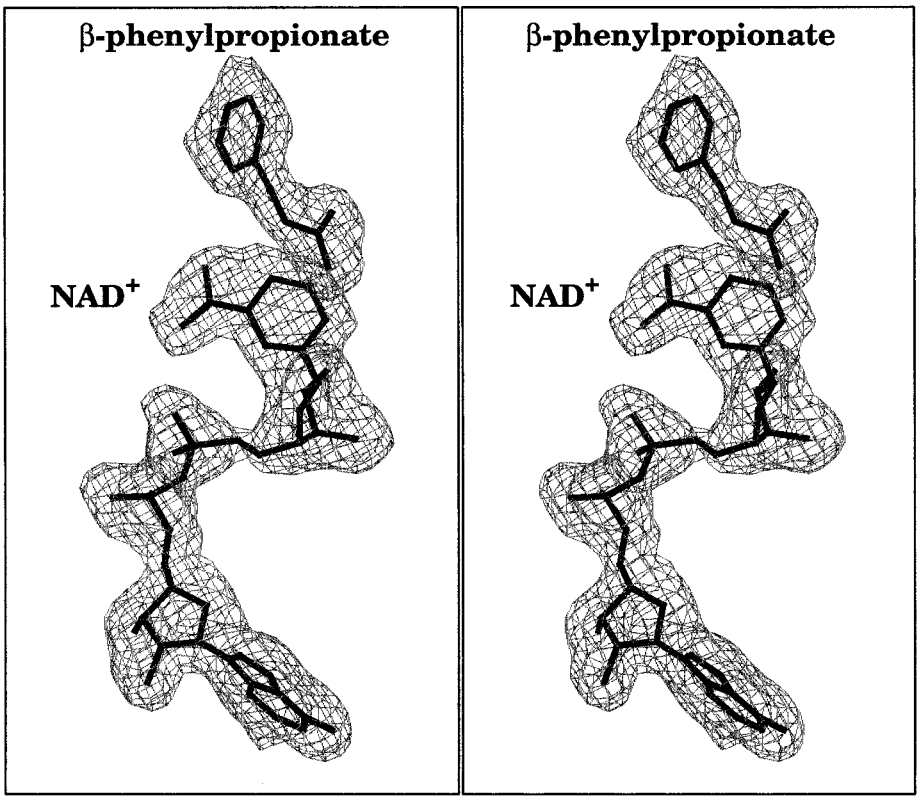

(b)

FIGURE 4: Representative electron density for the dinucleotides and the ligands. The maps shown were calculated with coefficients of the form ($F_o - F_c$), where F_o was the native structure factor amplitude and F_c was the calculated structure factor amplitude from the models lacking the coordinates for the dinucleotides and the ligands. (a) Electron density corresponding to NAD^+ and phenylpyruvate. The map was calculated with X-ray data from 30 to 1.5 Å resolution and contoured at 3σ. (b) Electron density corresponding to NAD^+ and β-phenylpropionate moieties. The map was calculated with X-ray data from 30 to 2.3 Å resolution and contoured at 3σ.

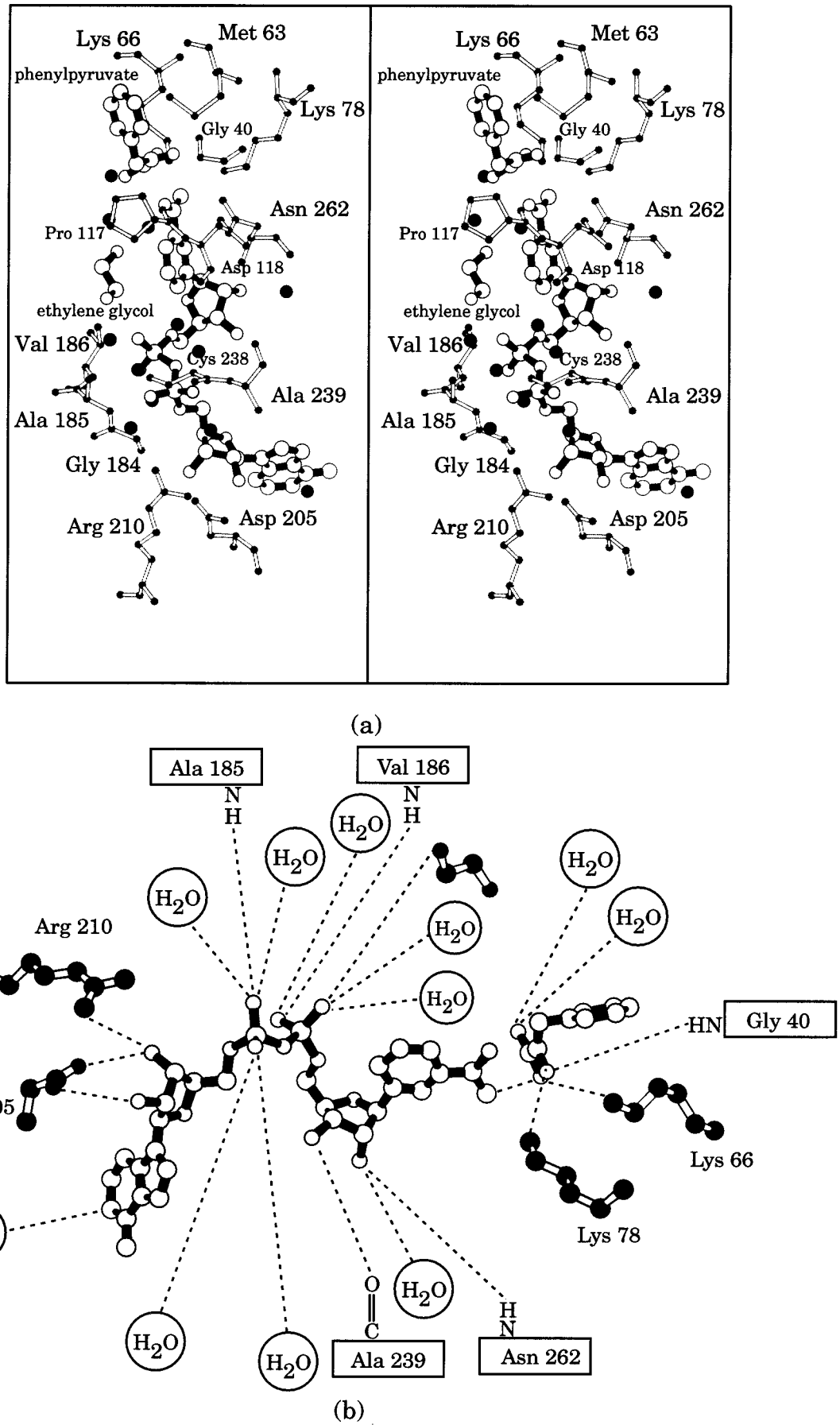

FIGURE 5: Active site for the phenylalanine dehydrogenase·NAD^+·phenylpyruvate ternary complex. Those amino acid residues located within approximately 3.2 Å of the dinucleotide and the ligand are displayed in panel a. A cartoon indicating potential hydrogen-bonding interactions between NAD^+, phenylpyruvate, and the protein is shown in panel b. Potential hydrogen-bonding interactions within approximately 3.0 Å are indicated by the dashed lines.

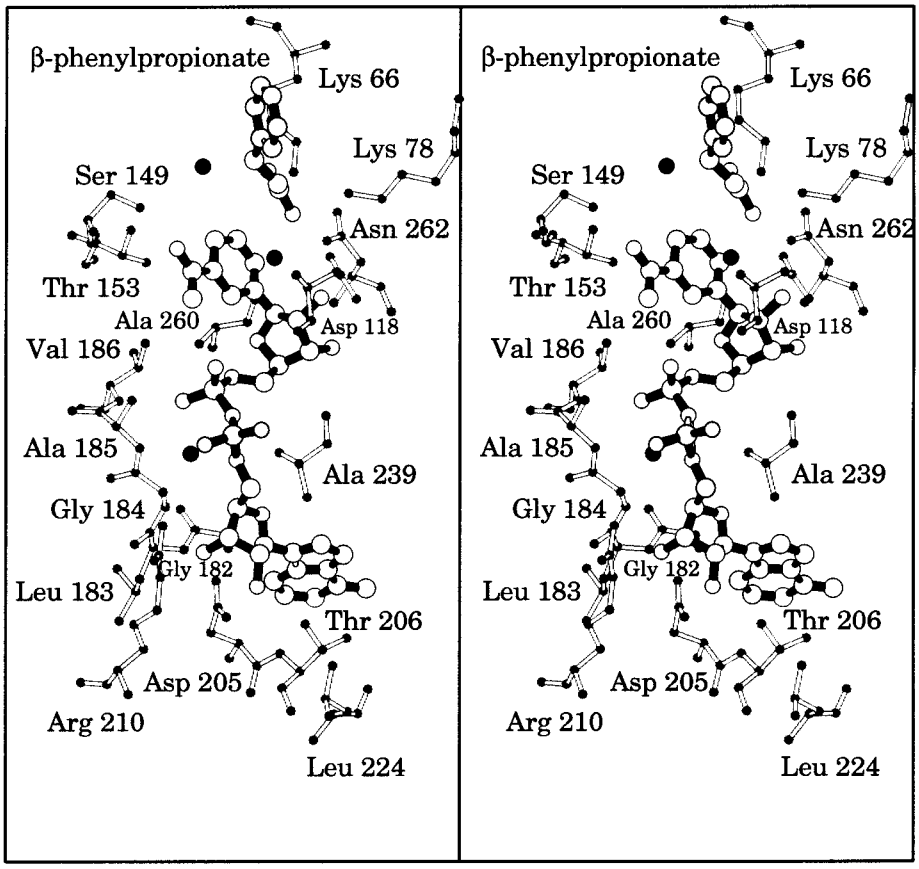

(a)

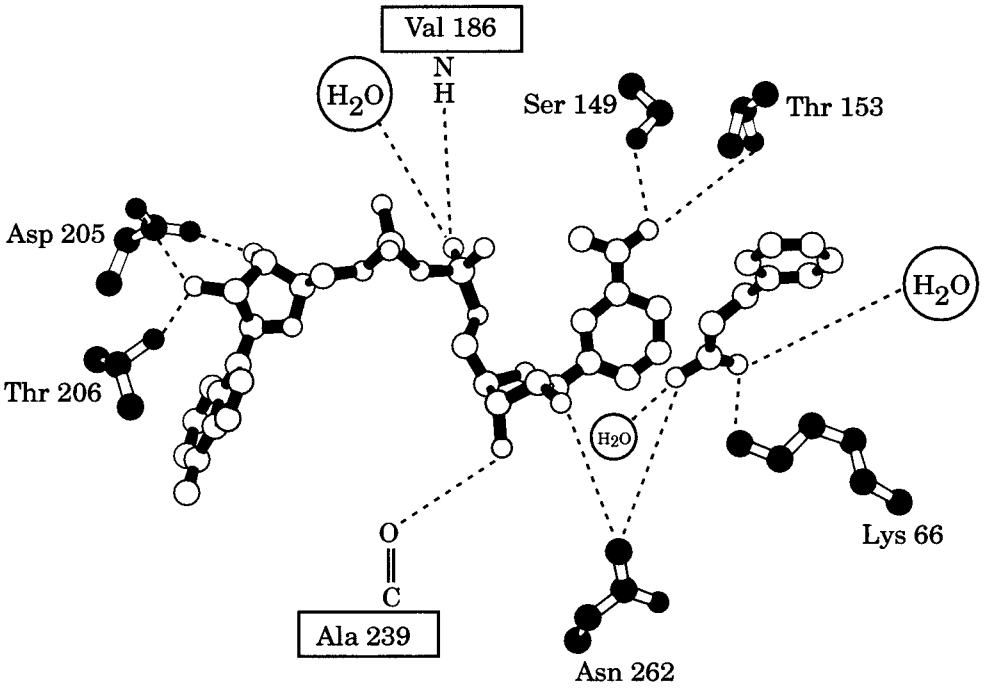

(b)

FIGURE 6: Active site for the phenylalanine dehydrogenase·NAD^+·β-phenylpropionate ternary complex. Those amino acid residues located within approximately 3.2 Å of the dinucleotide and the ligand are displayed in panel a. A cartoon indicating potential hydrogen-bonding interactions between NAD^+, β-phenylpropionate, and the protein is shown in panel b. Potential hydrogen-bonding interactions within approximately 3.0 Å are indicated by the dashed lines.

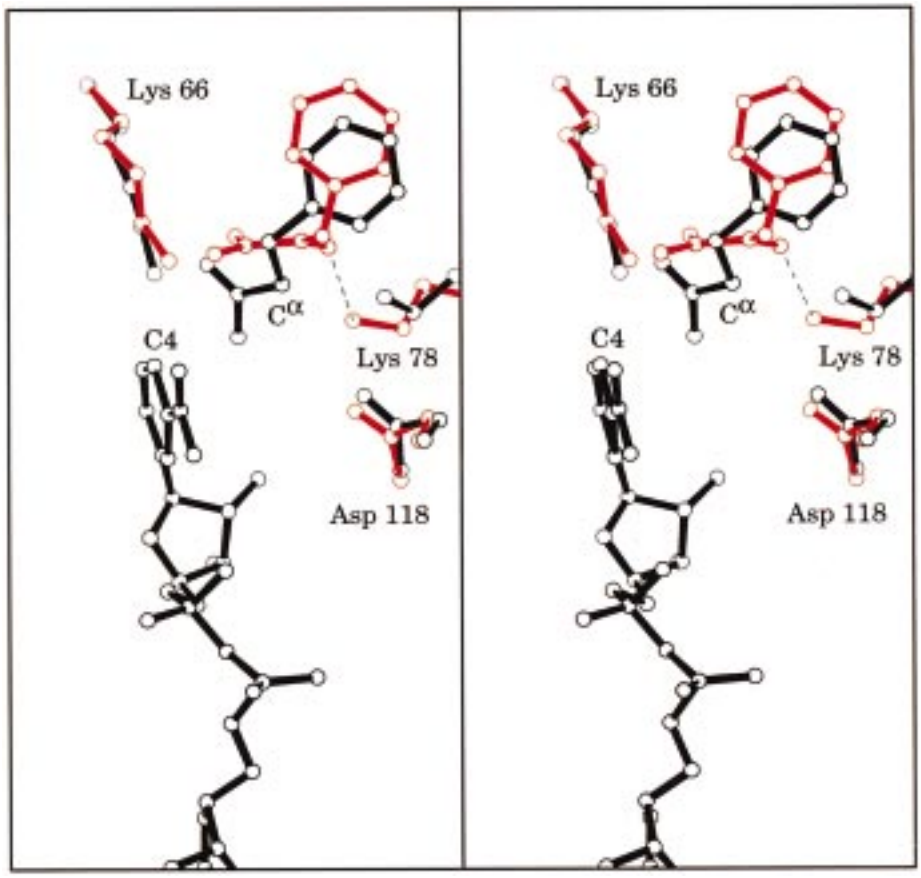

FIGURE 7: Closeup view highlighting the differences in ligand binding between the two inhibitory ternary complexes. Those residues and ligands corresponding to the enzyme·NAD^+·phenylpyruvate model and the enzyme·NAD^+·β-phenylpropionate complex are depicted in red and black, respectively. For the sake of clarity, the dinucleotide in the enzyme·NAD^+·phenylpyruvate model was omitted. The hydrogen bond of length 3.1 Å between the keto oxygen of phenylpyruvate and N^{ϵ} of Lys 78 is indicated by the dashed line.

between the dinucleotide and the protein that are significantly different from those observed in the phenylalanine dehydrogenase·NAD^+·phenylpyruvate ternary complex, as can be seen in Figure 6, panels a and b. In the enzyme·NAD^+·β-phenylpropionate complex, both O^{γ} of Thr 153 and O^{γ} of Ser 149 hydrogen bond with the carboxamide oxygen of the dinucleotide as indicated in Figure 6b, interactions that are not observed in the enzyme·NAD^+·phenylpyruvate species. Additionally, the C4 of the nicotinamide ring in this model now lies within 4.2 Å of C^{α} of the ligand and the nicotinamide ring is now in the proper orientation for the correct *B*-side-specific hydride transfer to the ligand, assuming that the binding position of the β-phenylpropionate mimics that of iminophenylpyruvate (the intermediate species reduced by NADH in the reaction mechanism). This distance of 4.2 Å is similar to that observed in UDP-galactose 4-epimerase, which transfers the 4S hydride from NADH to a 4′-ketopyranose intermediate thereby yielding either UDP-glucose or UDP-galactose (*19*).

Since the X-ray data for this structural analysis were collected at −3 °C without cryo-protectants, there are no ethylene glycol molecules in the active site. The active site for the phenylalanine dehydrogenase·NAD^+·β-phenylpropionate complex contains only three well-ordered water molecules positioned within 3.2 Å of the dinucleotide and the β-phenylpropionate, and as is obvious, the interactions between the dinucleotide and the protein are less extensive. There is an important difference in ligand binding between the two ternary complexes presented here. Due to the difference in orientation of the β-phenylpropionate versus phenylpyruvate, Lys 78 moves out of the 3.2 Å cutoff employed to define the active site. As such, N^{ϵ} of Lys 78 no longer hydrogen bonds with the ligand. This movement has important biochemical and enzymological implications as described in the following Discussion.

DISCUSSION

On the basis of their pH studies with bovine liver glutamate dehydrogenase, Rife and Cleland (*20*) proposed that the reductive amination of α-ketoglutarate to glutamate proceeds with the attack of neutral ammonia on the glutamate dehydrogenase·α-ketoglutarate complex to yield a carbinolamine intermediate. Subsequent elimination of water from this carbinolamine yields iminoglutarate, which is stereospecifically reduced by NAD(P)H to L-glutamate. Rife and Cleland's studies suggested that two enzymatic groups, possibly a lysine and a carboxyl-containing side chain, were involved in the proton-transfer events necessary to carry out the chemical transformations. The existence of the intermediates was subsequently verified, and the mechanism was extended by the investigations of Fisher and co-workers (*21*−*24*). The X-ray crystal structure of the *C. symbiosum* glutamate dehydrogenase in a binary complex with glutamate provided the first structural evidence for the participation of a lysine (Lys 125) and an aspartate (Asp 165) in the catalytic mechanism of the enzyme (*4*).

While the currently accepted chemical mechanism for glutamate dehydrogenase provides an elegant description of

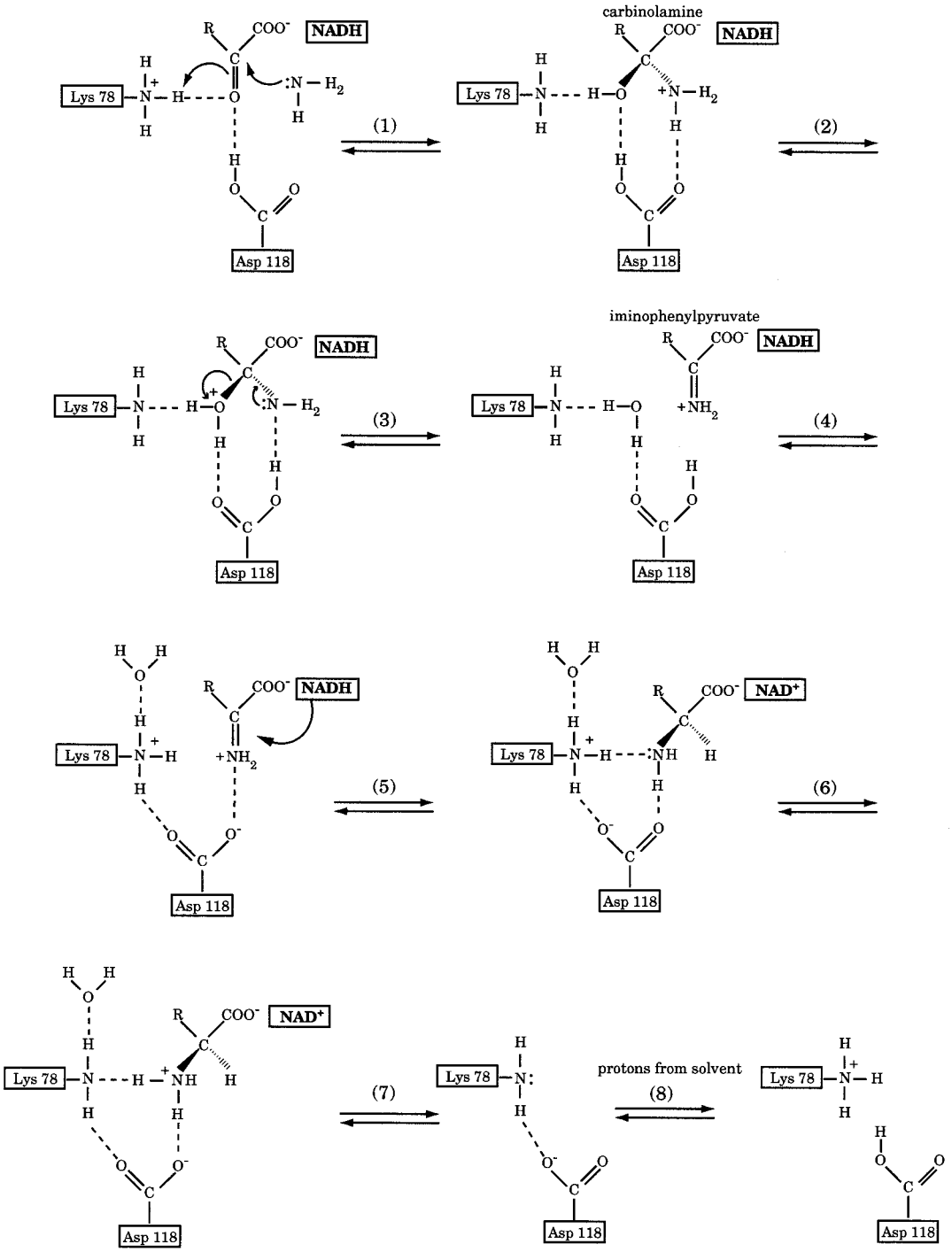

FIGURE 8: Revised chemical mechanism for phenylalanine dehydrogenase. The catalytic mechanism presented here is in the direction of phenylalanine synthesis from phenylpyruvate.

the chemical events that transpire during catalysis, it fails to adequately address a very important question, namely why the amino acid dehydrogenases do not simply catalyze pyridine nucleotide-dependent reduction of bound α-keto acids to 2-hydroxy acids. None of the previously reported structural analyses of these enzymes has furnished an explanation for the chemical specificity of the catalyzed reaction, not even the recently reported X-ray analysis of alanine dehydrogenase, whose pyruvate-binding site is structurally very similar to that of L-lactate dehydrogenase (*7*). The structures of the inhibitory ternary complexes of phenylalanine dehydrogenase reported here provide a convincing rationale for the discrimination between imino and keto acids as substrates for reduction by these dehydrogenases, and we use this rational to revise the current chemical mechanism of the enzymatic reaction.

Figures 5 and 6 detail the active-site interactions within the ternary complexes of phenylalanine dehydrogenase with NAD^+ and phenylpyruvate and NAD^+ and β-phenylpropionate, respectively. The dramatic difference in the orientation of phenylpyruvate versus β-phenylpropionate within the active site is highlighted in Figure 7.

In the enzyme·NAD^+·phenylpyruvate complex, the orientation of the pyridine nucleotide is such that direct hydride transfer to the phenylpyruvate (were the nucleotide NADH) cannot occur. Rotation of the nicotinamide moiety within

the active site to permit direct hydride transfer to the keto acid yields a distance of greater than 6 Å between C4 of the nicotinamide and the keto carbon of phenylpyruvate, which makes hydride transfer to phenylpyruvate highly improbable. As indicated in Figure 7, the keto oxygen of phenylpyruvate is hydrogen bonded to N^{ϵ} of Lys 78 in this model, and this interaction functions to draw the keto carbon away from the pyridine nucleotide, thus preventing a reaction between them.

The structure of phenylalanine dehydrogenase complexed with NAD^+ and the competitive inhibitor β-phenylpropionate clearly reveals positions for the nicotinamide ring and the inhibitor that are significantly different from those observed in the ternary complex with NAD^+ and phenylpyruvate. The orientations of the molecules are now better suited for hydride transfer, with a distance of 4.2 Å between C4 of the nicotinamide ring and C^{α} of β-phenylpropionate. The change in orientation of the nicotinamide moiety in this structure is quite dramatic, but is easily accommodated by the large active site with only a few perturbations in the positions of the surrounding amino acid residues. The hydrogen-bonding interaction to Lys 78 that is observed with phenylpyruvate is not available in the presence of β-phenylpropionate, and the loss of this interaction permits β-phenylpropionate to occupy a position much closer to the nicotinamide ring. The imine of phenylpyruvate can be modeled into this same position, and upon so doing a favorable electrostatic interaction between the positively charged imine nitrogen and the carboxylate of nearby Asp 118 is easily envisioned. Direct hydride transfer to iminophenylpyruvate would be expected to occur and yield L-phenylalanine as the amino acid product.

The enzymatic discrimination between imino and keto acids as substrates for reduction is thus a consequence of the hydrogen-bonding and electrostatic interactions of the substrate and intermediates with Lys 78 and Asp 118. Structural analyses of enzyme·NAD^+·L-phenyllactate and enzyme·NADH·L-phenylalanine complexes are currently being pursued to discern the manner in which the enzyme discriminates between amino and hydroxy acids as substrates for oxidation. A mechanism for the enzymatic transformation of phenylpyruvate to L-phenylalanine that incorporates the interactions observed in the present structures is presented in Figure 8. As shown in this scheme, phenylpyruvate is bound to the enzyme with its keto oxygen in hydrogen-bonding distance of the active-site lysine. This interaction prevents reduction of phenylpyruvate by NADH. In step 1, phenylpyruvate is attacked by neutral ammonia, and the active-site lysine donates a proton to the keto oxygen to yield a carbinolamine with a positively charged amino group. Proton transfer, assisted by the active-site carboxyl group, shifts this positive charge to the hydroxyl group of the carbinolamine in step 2. Water is subsequently eliminated from the carbinolamine in step 3, generating the second intermediate, positively charged iminophenylpyruvate. These first three steps are the same as those proposed by Rife and Cleland for glutamate dehydrogenase. In the next step of the glutamate dehydrogenase mechanism, the imine is reduced to an amino group by the pyridine nucleotide, and this amino group is subsequently protonated by the active-site carboxyl group. In the mechanism presented here for phenylalanine dehydrogenase, however, there is additional proton transfer from the carboxyl group of Asp 118 to Lys 78 following the elimination of water (step 4), which allows the now negatively charged Asp 118 to stabilize the positive charge on the imine and position this imine for hydride transfer. After reduction of iminophenylpyruvate by NADH (step 5), the amino group of phenylalanine is protonated by Lys 78 before its release from the active site. The protonation states shown for the reactants at the beginning and end of the reaction are consistent with the pH-dependent kinetic data of N.M.W. Brunhuber and J.S. Blanchard (manuscript in preparation).

The structures of these ternary complexes definitively establish that the keto acid substrate is juxtaposed between the pyridine nucleotide and the catalytic lysine, as postulated in the mechanism of Rife and Cleland. With such an arrangement, the attack of the ammonia and the hydride occurs from the same side, and the elimination of water is from the opposite side, assisted by its interaction with Lys 78 and Asp 118. In the mechanism presented here, the active-site water molecule is not expelled from the local region upon its elimination from the carbinolamine; instead, it remains in close proximity via a hydrogen-bonding interaction with Lys 78. This arrangement is purely speculative since this water is not observed in either of the models described here. However, it is consistent with the observation of an ordered water molecule bound to the catalytic lysine in the structure of the glutamate dehydrogenase·glutamate complex (*4*). We expect, on the basis of our proposed mechanism, to observe this ordered water molecule in the structure of the phenylalanine dehydrogenase·NADH·L-phenylalanine complex. Experiments designed to test this hypothesis are presently underway.

ACKNOWLEDGMENT

We thank Dr. W. W. Cleland for his insightful comments concerning the catalytic mechanism of phenylalanine dehydrogenase and for his critical reading of this manuscript.

REFERENCES

1. Brunhuber, N. M. W., and Blanchard, J. S. (1994) *Crit. Rev. Biochem. Mol. Biol. 29*, 415−467.
2. Baker, P. J., Britton, K L., Engel, P. C., Farrants, G. W., Lilley, K. S., Rice, D. W., and Stillman, T. J. (1992) *Proteins: Struct., Funct., Genet. 12*, 75−86.
3. Rossmann, M. G., Liljas, A., Brändén, C. I., and Banaszak, L. J. (1975) *The Enzymes*, 3rd ed., Vol. 11, 62−102.
4. Stillman, T. J., Baker, P. J., Britton, K. L., and Rice, D. W. (1993) *J. Mol. Biol. 234*, 1131−1139.
5. Baker, P. J., Turnbull, A. P., Sedelnikova, S. E., Stillman, T. J., and Rice, D. W. (1995) *Structure 3*, 693−705.
6. Scapin, G., Reddy, S. G., and Blanchard, J. S. (1996) *Biochemistry 35*, 13540−13551.
7. Baker, P. J., Sawa, Y., Shibata, H., Sedelnikova, S. E., and Rice, D. W. (1998) *Nat. Struct. Biol. 5*, 561−567.
8. Brunhuber, N. M. W., Banerjee, A., Jacobs, W. R., Jr., and Blanchard, J. S. (1994) *J. Biol. Chem. 269*, 16203−16211.
9. Kabsch, W. (1988) *J. Appl. Crystallogr. 21*, 67−71.
10. Kabsch, W. (1988) *J. Appl. Crystallogr. 21*, 916−924.
11. Rossmann, M. G. (1960) *Acta Crystallogr. 13*, 221−226.
12. Terwilliger, T. C., and Eisenberg, D. (1983) *Acta Crystallogr., Sect. A 39*, 813−817.
13. Bricogne, G. (1976) *Acta Crystallogr., Sect. A. 32*, 832−847.
14. Tronrud, D. E., Ten Eyck L. F., and Matthews, B. W. (1987) *Acta Crystallogr., Sect. A 43*, 489−501.
15. Kleywegt, G. J., and Jones, T. A. (1997) *Methods Enzymol. 277*, 525−545.
16. Lee, B., and Richards, F. M. (1971) *J. Mol. Biol. 55*, 379−400.

17. Thoden, J. B., Frey, P. A., and Holden H. M. (1996) *Protein Sci. 5*, 2149−2161.
18. Thoden, J. B., Frey, P. A., and Holden, H. M. (1996) *Biochemistry 35*, 2557−2566.
19. Thoden, J. B., and Holden, H. M. (1998) *Biochemistry 37*, 11469−11477.
20. Rife, J. E., and Cleland, W. W. (1980) *Biochemistry 19*, 2328−2333.
21. Srinivasan, R., and Fisher, H. F. (1985) *Biochemistry 24*, 618−622.
22. Fisher, H. F., Pazhanisamy, S., and Medary, R. T. (1987) *J. Biol. Chem. 262*, 11684−11687.
23. Srinivasan, R., Viswanathan, T. S., and Fisher, H. F. (1988) *J. Biol. Chem. 263*, 2304−2308.
24. Fisher, H. F., Maniscalco, S., Singh, N., Mehrotra, R. N., and Srinivasan, R. (1992) *Biochim. Biophys. Acta. 1119*, 52−56.

BI982244Q